REAL TIME MODELING OF ACOUSTIC PROPAGATION IN COMPLEX ENVIRONMENTS

Fabio Antonacci, Marco Foco, Augusto Sarti, Stefano Tubaro

Dipartimento di Elettronica e Informazione - Politecnico di Milano
Piazza L. Da Vinci 32 - 20133 Milano, Italy
`{antonacci|foco|sarti|tubaro}@elet.polimi.it`

ABSTRACT

In order to achieve high-quality audio-realistic rendering in complex environments, we need to determine all the acoustic paths that go from sources to receivers, due to specular reflections as well as diffraction phenomena. In this paper we propose a novel method for computing and auralizing the reflected as well as the diffracted field in 2.5D environments. The method is based on a preliminary geometric analysis of the mutual visibility of the environment reflectors. This allows us to compute on the fly all possible acoustic paths, as the information on sources and receivers becomes available. The construction of a beam tree, in fact, is here performed through a look-up of visibility information and the determination of acoustic paths is based on a lookup on the computed beam tree. We also show how to model diffraction using the same beam tree structure used for modeling reflection and transmission.

In order to validate the method we conducted an acquisition campaign over a real environment and compared the results obtained with our real-time simulation system.

1. INTRODUCTION

Finding all the paths that link a source and a receiver in a complex environment using the laws of geometric reflection is a problem of crucial importance in a variety of applications ranging from realistic sound rendering to the modeling of indoor multipath fading in electromagnetic propagation. Several methods have been proposed for a fast determination of paths in both 3D and 2D space [1]. In particular, the beam tracing method [2] proved to be one of the most efficient solutions for determining such paths. One interesting aspect of this approach is that, given the location of the source, we can pre-compute the branching topology of all beams that propagate from that source through the construction of a data structure called *beam tree*. If we consider a receiver placed in any point in space, we can then quickly determine (through beam-tree lookup) which beams pass through that point and retrieve all the information that is needed to rapidly construct the paths between source and receiver. In conclusion, given a source location, this approach allows us to determine very quickly how the paths change as receiver moves. On the other hand, the beam tree depends on the reflectors' configuration as well as the source location, therefore every time we move the source, we need to recompute it. This operation can be rather costly, as it needs us to re-evaluate the visibility from the new source location.

A solution to this problem was recently proposed in [4]. The idea behind that method was to first compute the visibility information on the environment (reflectors) from an arbitrary point in space, which is equivalent to the visibility of a generic reflector from a point on a generic reflector. This information is computed and stored in a specific data structure in a preliminary analysis phase. As soon as we specify the source location, we can then iteratively construct the beam tree through lookup of the visibility information. As soon as we specify the receiver's location, we can iteratively determine the paths between source and receiver through beam tree lookup. A clever arrangement of the visibility information based on visibility diagrams (defined in the dual of the geometric space) enables a fast update of the beam-tree, which means that both sources and receivers can move in the environment during the auralization process.

In this paper we propose a method that extends this approach in such a way to model diffraction as well as geometric reflections. In particular, we extend the concept of visibility diagram in order to account for the diffracted field. We assume that the acoustic environment is 2.5D (vertical walls perpendicular to floor and ceiling). This allows us to simplify the analysis of 3D acoustic propagation and visualize it on a 2D floor plan. The approach that we propose, however, can be generalized to the case of a full-3D environment.

Diffraction is a fundamental mode of propagation in densely occluded environments. As a matter of fact, if source and receiver are not in direct visibility (and the transmission of sound through walls is negligible), then the first significant acoustic arrival will follow the shortest diffracted path.

In general, the diffracted field tends to enhance the spatial impression of the environment in which the receiver is immersed. In order to account for it, we consider a geometric approximation of the diffracted field based on the addition of a virtual source on each diffractive wedge. The diffractive paths can thus be thought of as "geometric Fermat paths" passing from a point on the diffractive edge. We will show that these edges, in our 2.5D approximations, are points on the floor plan, therefore diffractive paths are modeled as paths passing through this point. For this reason, we can pre-compute a beam tree for every potentially diffractive point in the map and use this propagation tree in runtime to evaluate diffracted propagation paths. Given these diffractive paths, in this paper we propose three different methods for simulating the diffractive effect with different computational loads.

We also show the results of some validation tests conducted in a real office environment. The tests consist of comparing some descriptors of the estimated impulsive response with the measured one.

This paper is organised as follows: in Section 2 we illustrate

the key concept of visibility diagram. In Section 3 we describe the extension of the visibility diagram in order to account for diffraction; Section 4 describes the methods used for measuring the impulse response of a room; finally Section 5 shows the results of the validation tests.

2. VISIBILITY DIAGRAMS

One key concept behind our work is the visibility diagram, which is a parameter-space representation of the visibility between reflectors. The visibility function of a reflector from an arbitrary viewpoint is here defined as a boolean function of the plenoptic space (the parametric space that describes a ray that departs from a generic point in space in an arbitrary direction). This function tells us whether or not the reflector will be visibile from that viewpoint while looking in the considered direction. A two-dimensional plenoptic space is thus described by three parametres: two for the viewpoint location and one for the viewing angle. Notice, however, that all points on a visual ray share the same value of the visibility function. This tells us that a plenoptic parametrization is, in fact, redundant. This fact is well known in applications of image-based rendering, where the plenoptic space is often replaced by a reduced-dimension space (see, for example, the Lumigraph [3]). In our case this dimensionality reduction can be easily achieved by considering only the viewpoints that lie on a reference section of the geometric space (a reference line in 2D environments and a reference plane in the 3D case). This section, in principle, can be chosen arbitrarily, as long as it does not lie on the reflector whose visibility we are evaluating. It is important to remember that the visibility function will be iteratively looked up for tracing beams in the geometric space, therefore it is important to choose the reference section in such a way to simplify this process. We will see that this can be achieved by making the reference section coincide with another reflector. This corresponds to defining the visibility *of* a reflector *from* another reflector. A complete evaluation of the environment visibility is thus given by the whole collection of visibility functions of all reflectors from all reflectors.

With reference to Figs. 1 and 2, the visibility of reflector 2 from reflector 1 can be expressed as a boolean function of two parameters q and $m = \tan\phi$. This function indicates whether a visual ray in position q on reflector 1 pointing in the direction ϕ passes through any point of reflector 2. Notice that the visibility region on the plane (m, q) corresponds to the dual of the reflector 2 with respect to a reference frame attached to reflector 1.

Let us consider the visibility diagram of reflector r_1 in Figure 1, which describes how the other reflectors are seen from viewpoints on r_1. The first step consists of choosing a reference frame attached to r_1, which is normalized in such a way that r_1 will correspond to the segment (x_1, y_1), with $x_1 = 0$ and $-1 \le y_1 \le 1$. This choice allows us to delimit the parameter space to the reference strip corresponding to $-\infty \le m \le \infty$ and $-1 \le q \le 1$ (dual space of the reference reflector).

The rays departing from the reference segment and hitting the other segments correspond in the (m, q) space with visibility regions, for example the visibility region of s_2 is showed in Figure 2.

Considering the dual space interpretation, the visibility regions of the various reflectors with respect to the reference one can be computed in closed form [4]. Notice, however, that the visibility regions of the various reflectors overlap in regions corresponding to visual rays that intersect more than one reflector. Figuring out
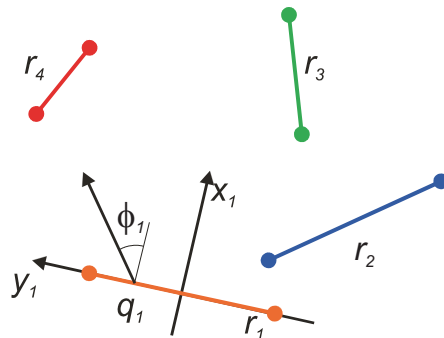

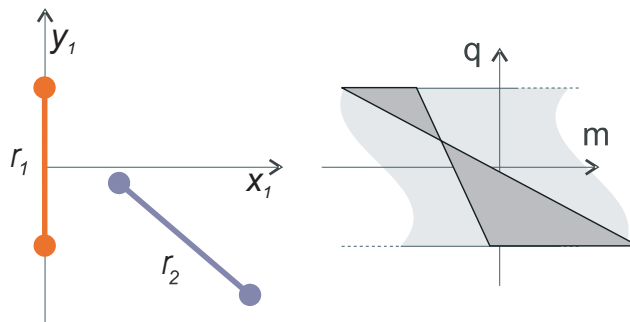Figure 1: *2D Environment to be used for the illustration of the visibility diagram construction process.*

Figure 2: *Visibility region corresponding to segment s_2.*

which reflector occludes which corresponds to sorting out which regions overlaps which. This ordering operation can be performed very quickly by back-tracing one ray for each connected overlapping area. Once overlaps are all sorted out, the visibility of environment of Figure 1 from reflector 1 is shown in Figure 3.
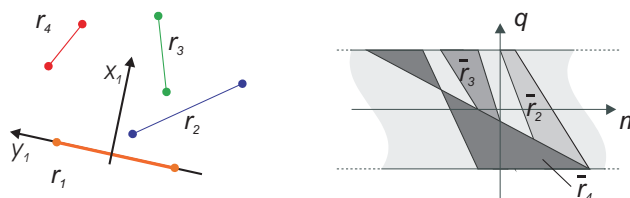

Figure 3: *Environment geometry (left-hand side) and visibility diagram of the s_1 segment. The visibility regions of the various reflectors are here shown with different colors.*

Visibility diagrams can all be computed in a pre-analysis phase, and this information can be used for a fast construction of a beam tree and a fast determination of all geometric paths between source and receiver. As soon as the source location is specified, the initial beam departing from it will split into a number of sub-beams, each inciding on a different reflector. The reflected beams will then branch out again as they reach other reflectors. In order to trace all such reflections and branchings, we can implement an iterative process that involves looking up visibility information.

At the generic step of the branching process, a beam is characterized by a (real or virtual) source and that portion of a reflector

that is "illuminated" by the beam (active portion of the reflector). The visibility from the active portion of the reflector can be readily obtained from the visibility of the whole reflector by narrowing the reference strip in the parameter space. Similarly, all the rays that depart from a source location correspond to a line on the visibility diagram (we recall that the parameter space of the visibility diagram is, in fact, the dual of the geometric space). The beam will thus be the intersection between the narrowed reference strip (illuminated portion of the reflector) and the dual line corresponding to the source (set of all visual rays that depart from the source's origin). In conclusion, in order to determine which reflectors the beam will encounter in its path after being reflected by r_i, we just need to determine the intersection between the dual of the source (a line) and the visibility regions of all the reflectors as seen from r_i.

Once the beam tree is constructed, all paths corresponding to a given receiver location can be readily found through a simple beam tree lookup as described in [4] and [2].

3. ALGORITHM

As already mentioned above, in a 2.5D environment all diffractive edges are can be visualized as points on the floor plan as we assume that all diffractive edges are vertical. In order to render the diffracted field, we use the *Uniform Theory of Diffraction* (*UTD*), which models diffraction by placing a virtual source on each diffractive wedge. In practical cases, the UTD is not used when the diffractive edge is not long enough, as the diffractive field would in this case be negligible.

In order to render the diffracted field the very first phase of the proposed algorithm consists of the diffractive wedge selection. In facts not all the wedges in the environment can obscure the line of visibility path between source and receiver.
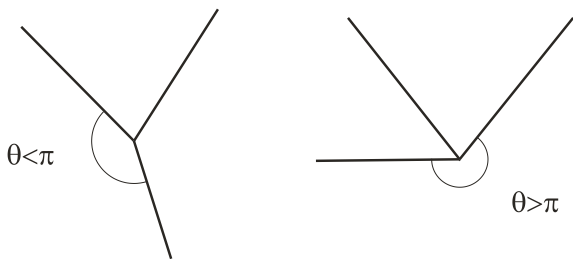
Figure 4: *Two examples of wedges, the hand-left side one will not be considered a diffractive wedge, while the right-hand side one will be considered a diffractive wedge.*

After selecting the diffractive wedge we trace two beam trees from a virtual source placed on the diffractive edges (see Figure 5): the first-level beams will be traced in the two regions marked as **I** and **II**.

At this point, the first level beams follow a reflection procedure that is completely similar to a regular beam tracing approach based on visibility diagram [4]. The depth of the diffractive beam tree must be determined in a different fashion compared to reflective beam trees for reasons of relevance and computational load. This operation can be done in a pre-computation phase, i.e. without knowing source and receiver positions. Once the diffracted beam trees are traced, we only need to test source and receiver positions in the two previously computed beam trees in order to
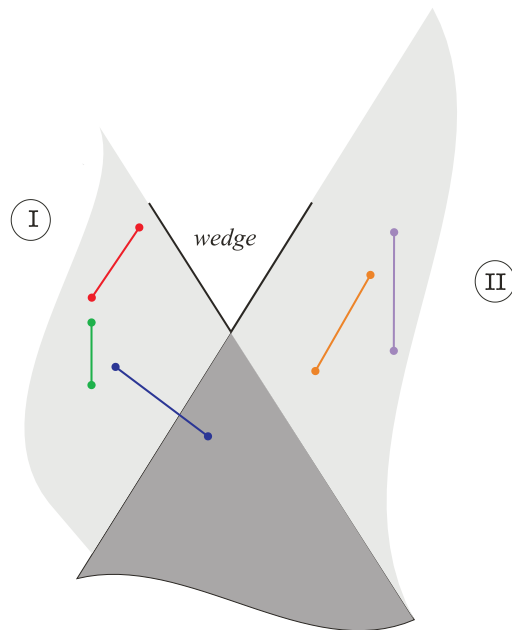
Figure 5: *An example of a diffractive wedge and the angular regions in which the first-level beams will span in the beam tracing execution.*

obtain all paths between source and diffractive wedge and from the diffractive wedge to the receiver.

3.1. Rendering the diffracted field

In order to render the diffracted field we propose three approaches. The first rendering technique is based on the computation of a filter for every diffractive path using the *Uniform Theory of Diffraction (UTD)*. The second approach sacrifices some of the accuracy in exchange of a reduction of computational complexity. In fact, in most of the applications of virtual acoustics we are more interested in producing a convincing sound rather than a physically-accurate one. A simplified method is based on a double interpolation. In particular, during a precalculation phase we record the complex value of the diffracted field at the origin of the beam ("penumbra" area) and in proximity of the wall in the shadow region. This operation is done by placing the source at eight angles in the angular range where the beam tree spans and for eight frequencies between 0 and $3\,\text{kHz}$. The source-wedge and receiver-wedge distances are assumed to be the half the distance between unoccluded walls. We use this information in the calculation phase as follows: we first check that source and receiver fall in the beam trees departing from the considered wedge; we calculate then the complex-value of the diffracted field of penumbra and shadow zone as linear interpolation of nearest values in the precalculated structure. The interpolation is angle-based. Let $D_{f,h}(\beta_i)$ and $D_{f,h}(\beta_{i+1})$ be the magnitude of the diffracted penumbra field at two of eight angles that lie the closest to the source (whose angle with the closest side of the wedge is β_s) and at frequency f. The first interpolation is

$$D_{f,h}(\beta_s) \approx D_{f,h}(\beta_i)\frac{\beta_{i+1}-\beta_s}{\beta_{i+1}-\beta_i} + D_{f,h}(\beta_{i+1})\frac{\beta_s-\beta_i}{\beta_{i+1}-\beta_i} \ .$$
(1)

The same interpolation is used for phase and magnitude of $D_{f,h}(\beta_s)$.

A similar relationship can be written for phase and magnitude of the diffracted field at the shadow zone, $D_{f,s}(\beta_s)$:

$$D_{f,s}(\beta_s) \approx D_{f,s}(\beta_i) \frac{\beta_{i+1} - \beta_s}{\beta_{i+1} - \beta_i} + D_{f,s}(\beta_{i+1}) \frac{\beta_s - \beta_i}{\beta_{i+1} - \beta_i} . \tag{2}$$

Given the position of the receiver, we use a linear angle-based interpolation between the penumbra and shadow values of the diffracted filter at the frequencies we are considering.

Let α_r be the angle between the wedge side that lies closest to the source and receiver. If α_1 and α_2 are the angles between the same segment and the beginning and the end of the lobe in which the receiver falls, then using the eqs. (1) and (2), the magnitude and the phase of the diffracted field at the receiver can be written as follows:

$$D_f(\alpha_r) \approx D_{f,s}(\beta_s) \frac{\alpha_r - \alpha_1}{\alpha_2 - \alpha_1} + D_{f,h}(\beta_s) \frac{\alpha_2 - \alpha_r}{\alpha_2 - \alpha_1} .$$

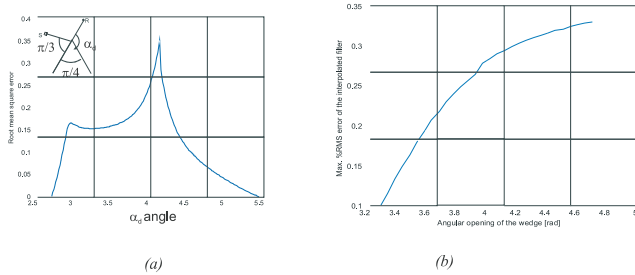An inverse Fourier transform is then computed in order to obtain the required filter.

(a) *(b)*

Figure 6: *RMS error of the diffracted filter for a $2\pi - \pi/4$ wedge as function of the receiver angle (left) and maximum RMs error as function of the wedge opening.*

In order to validate the double interpolation method and compare his computational complexity, we executed a comparison of the filter calculated using UTD and double interpolation techniques. In Figure 6 is shown the RMS error of the interpolated filter and the non interpolated filter, the RMS error is computed as follows:

$$E_{RMS}(\alpha_d) = \sqrt{\frac{\sum_n [h_d(n, \alpha_d) - h(n, \alpha_d)]^2}{\frac{1}{2} \sum_n [h_d(n, \alpha_d) + h(n, \alpha_d)]^2}} ,$$

where $h_d(n, \alpha_d)$ is the n-th sample of the interpolated filter when the receiver is placed at angle α_d, while $h(n, \alpha_d)$ is the n-th sample of the UTD filter at the same receiver position.

In the left-hand side of Figure 6 the wedge opening is $2\pi - \pi/4$ and, as expected, the maximum error takes place when the receiver is in the middle of the diffracted beam. In the implementation a wedge of such angular opening would not be auralized by UTD. In the right side of Figure 6 we plot the maximum RMS error moving the receiver in the middle of the diffracted beam for various angular openigns of the wedge itself. The larger the angular opening, the larger the interpolation error.

The third proposed approach renders the diffracted field using a sample for every diffracted path, with a RMS value that equals the RMS value of the diffractive filter.

4. MEASURING THE ACOUSTICAL IMPULSE RESPONSE

The aim of this Section is to validate the algorithm illustrated above. We compared synthetic parameters obtained from the computed impulse responses, with those computed from the measured impulse responses. The impulse responses were measured using a Maximum Length Sequence (MLS) as source and recording the corresponding signal with a condenser microphone. Let $h(n)$ be the impulse response (of length N) that we need to measure, $v(n)$ the MLS signal (of length M), and $y(n)$ the recorded signal. We can estimate the impulse response as

$$\widetilde{h}(n) = \sum_{m=0}^{M} y(n + m)v(m) . \tag{3}$$

If the acquisitions are corrupted by an environmental noise (of RMS value σ_n) that is incorrelated with the MLS signal, then the Signal to Noise Ratio obtained with this method is given by

$$SNR = \frac{M}{N} \sigma_n^2 . \tag{4}$$

The impulse response acquired with eq. (3) keeps trace of every transfer function encountered by the signal: D/A converter, speaker, environment, microphone and A/D converter. In order to reduce the impact of the transfer functions related to rendering and acquisition devices we implemented a deconvolution algorithm (details can be found in [5]). The algorithm uses the first echo as deconvolution element. Assuming that the air has no filtering effect on acoustic signal, an echo corresponding to the line of visibility path betweeen source and receiver will keep trace only of the transfer functions introduced by acquisition and output devices. A different situation can be devised when the direct signal between source and receiver is absent: in fact the first echo will correspond to the diffracted signal and will be filtered by the typical low-pass effect of diffractive propagation. The last task will be a high-pass filtering in order to lower the effect of electric interferences.

5. VALIDATION OF THE ALGORITHM

The floor plan of the testing environment is shown in Figure 7. The first test we conducted aims at comparing the simulated acoustical response with the acquired one. In this work we neglected propagation modes such as diffusion and late reverberations. In order to reduce the effect of such propagation modes we considered only the most energetic samples of the measured impulse response. The microphone position used in this first test is marked with **R**, while speaker position is marked with $\mathbf{S}_1$.

Our algorithm focuses on early reflections and low-order diffraction, therefore we will compare only the first part of the impulse respones.

As predicted, the first arrival of measured and simulated impulse responses (neglecting transmission by walls) comes from diffractive paths (marked in Figure 8 with the numerals **1** and **2**). Although the first arrival comes from diffractive path, the most energetic samples of the impulse responses correspond to reflective
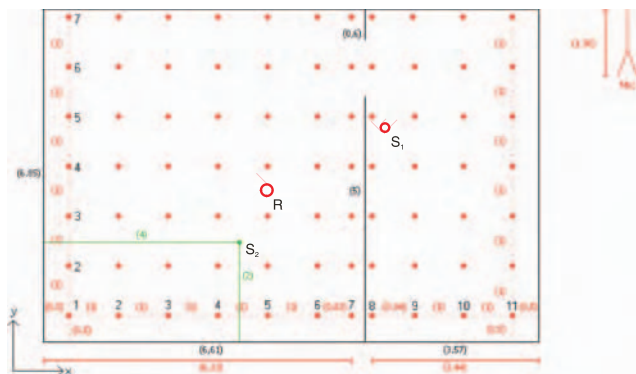
Figure 7: *Test environment: the microphone positions are marked with red points and speaker position is marked with green point.*
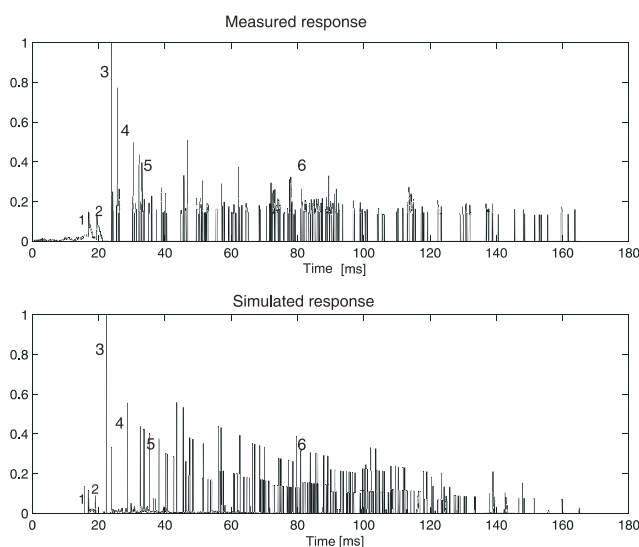

Figure 8: *Comparison of measured response (top) and simulated response (bottom).*

Figure 9: *A typical impulse response and the corresponding Schröder envelope.*

paths (marked in Figure 8 with the numerals **3, 4** and **5**). Finally, we notice a densification of the echoes in the last portion (marked with **6**) of the impulse response: this is the effect of high-order reverberation and in beam tracing algorithm these echoes are modelled by high-level beams in the beam tree data structure.

In order to compare simulation and acquisition results on a larger scale we had to properly choose the model parameters using the measured impulse responses. Several parameters can be computed from the envelope of the impulse response and a number of solutions are available in the literature. We adopted a method based on the Schröder integration, whose details can be found in [6].

Figure 9 shows a measured acoustic impulse response and the corresponding Schröder envelope. A typical Schröder envelope exhibits a first portion where the curve decays linearly, while the following portion dims down very rapidly. The temporal location of the Schröder curve's slope change can be taken as a measurement of the impulse length.

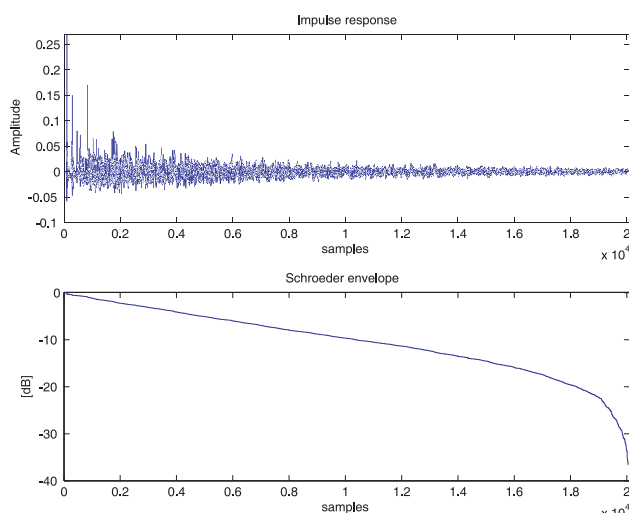Once we compute the Schröder envelope we can define several

parameters:

- Early Decay Time (EDT): the time where the Schröder envelope decays $10\,dB$ from original level. In literature the EDT is thought as the time where the early reflections are terminated.

- T15: the distance between the time where the value of the Schröder envelope is $-5\,dB$ and $-20\,dB$. Similarly we can define the T20 (decay from $-5\,dB$ to $-25\,dB$).

Other parameters can be defined directly from the impulse response:

- Centre time: it is the first order momentum of the squared pressure impulse response, starting from the arrival of the direct wave.

- Energy of the impulse response.

  In order to validate the algorithm, in this context we compared the Early Decay Time, and the centre time of measured, simulated with and without diffraction impulse responses.

In Figure 10 is shown the Early Decay Time of the measured (top) simulated with diffraction (centre) and without diffraction (bottom) impulse response in the test environment. From a visual comparison is clear that the simulated response using diffractive paths better approximates the measured response. In particular, we notice that the region near the door is not well represented in the absence of diffractive paths.

Figure 11 shows a comparison between the energy of the measured impulse response (top), that of the simulated response in presence of diffractive paths (centre) and in absence of diffractive paths (bottom). We notice that the presence of diffractive paths provides a better approximation of the measured response.
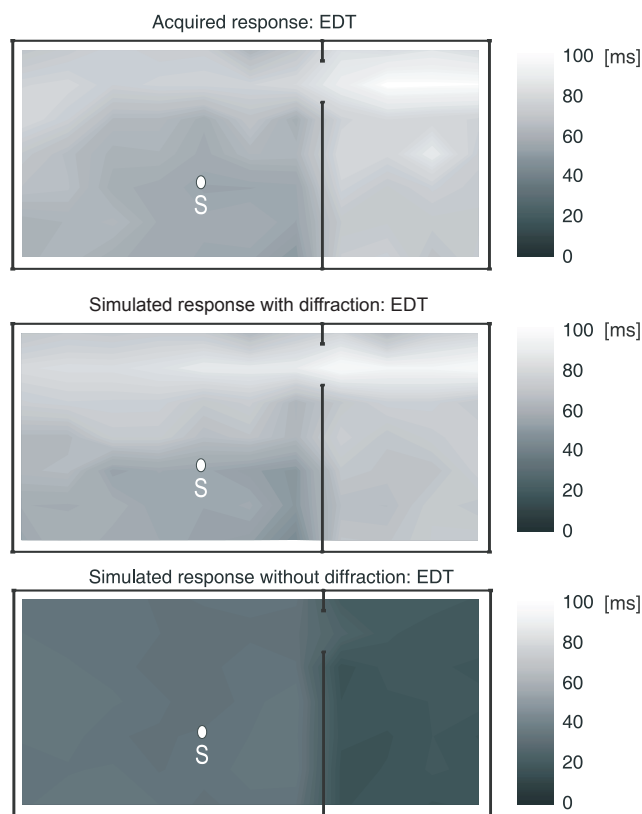
Figure 10: *Comparison of energy of measured (top), simulated with diffraction (centre) and without diffraction (bottom) responses. We can observe that the contrast between illuminated region and obscure region is smaller in presence of diffractive paths, approximating better the real situation.*

Figure 11: *Comparison of the centre time of measured (top), simulated with diffraction (centre) and without diffraction (bottom) impulse responses.*

6. CONCLUSIONS

In this paper we proposed a novel method for high-quality rendering of audio in complex 2.5D virtual environments. The method generalizes to the case of diffracted sound propagation a beam tracing method driven by visibility functions. The method proved to be able to produce realistic rendering of both the reflected and the diffracted acoustic field with a modest computational complexity. We also proposed alternative solutions that sacrifice accuracy in exchange of computational efficiency, which produce very convincing results.

7. REFERENCES

[1] A. Sarti, S. Tubaro, "Efficient geometry-based sound reverberation," *X EUSIPCO*, Toulouse, France, 2002.

[2] T. Funkhouser, I. Carlbom, G. Elko, G. Pingali, M. Sondhi, J. West, "Beam Tracing Approach to Acoustic Modeling for Interactive Virtual Environments," *Computer Graphics (SIGGRAPH '98)*, Orlando, FL, July 1998, pp. 21–32.

[3] S. J. Gortler, R. Grzeszczuk, R. Szeliski, M. F. Cohen, "The lumigraph," *23rd Intl. Conf. on Computer Graphics and Interactive Techniques - SIGGRAPH 1996*, New Orleans, Louisiana, USA, August 1996, pp. 43–54.
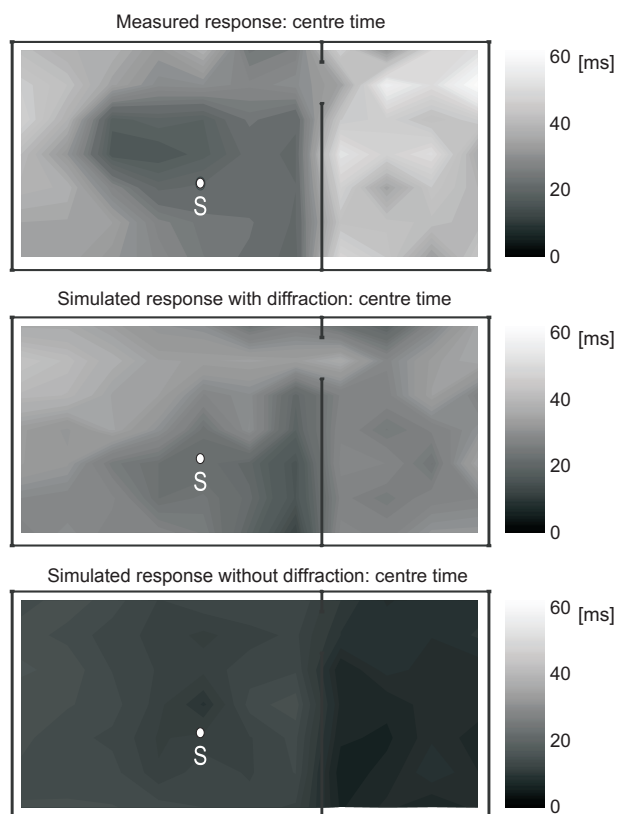
[4] M. Foco, P. Polotti, A. Sarti, S. Tubaro, "Sound Spazialitazion Based on Fast Beam Tracing in the Dual Space," *Proceedings of the COST G-6 Conference on Digital Audio Effects (DAFX-03)*, London, Great Britain, Sept. 2003.

[5] Z. Yao, G. F. Margrave, E. V. Gallant, "Optimal Spike Deconvolution and its Application in the Physical Model Measurement," *CREWES Research Report*, vol. 11, 1999.

[6] M. Karjalainen, P. Antsalo, A. Mäkivirta, T. Peltonen, V. Välimäki, "Estimation of Modal Decay Parameters from Noisy Response Measurements," *Journal of the Audio Engineering Society*, vol. 50, no. 11, Nov. 2002.